Korean J. Chem. Eng., 33(7), 1977-1988 (2016)
DOI: 10.1007/s11814-016-0064-z
pISSN: 0256-1115
eISSN: 1975-7220

INVITED REVIEW PAPER

Phase behavior of gas hydrates in nanoporous materials: Review

Daeok Kim and Huen Lee†

Department of Chemical & Biomolecular Engineering, Korea Advanced Institute of Science and Technology (KAIST), Daejeon 34143, Korea

(*Received 20 December 2015 • accepted 29 February 2016*)

Abstract−A precise understanding of phase behavior for a variety of both artificial and natural processes is essential to achieving scientific and technological goals. There has been growing research interest in gas hydrates confined in nanoporous media aiming to simulate and analyze the unique behavior of natural gas hydrates in sediments. Moreover, the appearance of peculiar properties due to the confinement effect stimulates research on gas hydrate technology for gas separation, such as CO_2 capture from versatile pre/post combustion emissions. In spite of their importance, reliable phase equilibrium data on gas hydrates confined at a nanoscale are scattered throughout the literature, while those in bulk state are abundant. Accordingly, we surveyed the previous studies on the phase behavior of gas hydrates in various nanoporous materials to include and provide valuable information and knowledge for start-up researchers in various gas hydrate fields.

Keywords: Gas Hydrate, Nanoporous Material, Phase Equilibria, Water, Confinement Effect

INTRODUCTION

Water, one of the simplest molecules in the world, has always been an objective of curiosity, and many studies have investigated its characteristics. The eagerness to understand water expanded research to a new field, the so-called clathrate hydrate, with the discovery of chlorine clathrate hydrate structure in 1810 by Humphry Davy [1]. Clathrate hydrates are unique inclusion compounds in which a small guest such as an atom, an ion or a gas molecule is enveloped in a host cage made of hydrogen-bonded water molecules at appropriate temperature and pressure conditions. The structure is called a gas hydrate when gas molecules are encaged as guests. The particular water-cage structures are maintained by the van der Waals force between the guest and host, which prevents the collapse of the host water frameworks. One of the most important features of a gas hydrate is that small molecules, ions and radicals can be stored in an ice-like structure [2-4]. To shed light on this phenomenon, many research efforts have been made to develop artificially synthesized clathrate hydrate cages for efficient gas storage and transportation of energy gases such as H_2 and CH_4 [5-7]. It is generally believed that a tremendous amount of natural gas is stored in the form of gas hydrate in permafrost regions and deep sea sediment, and this gas hydrate is considered to be a clean future energy source [8].

Contrary to such beneficial features, the formation of clathrate in transporting lines and the resulting plugging of pipes has been a major concern in oil and gas operation. To solve this problem, there have been many efforts to prevent the formation of the gas hydrate structure in terms of inhibition; the development of inhibitors (that is, materials designed to inhibit the formation or aggregation of gas hydrates) has been an active field in gas hydrate research [9,10]. Thus, gas hydrates are of great interest to both science and engineering disciplines.

Gas hydrate research has been extended to the nanoscale; the behavior of gas hydrates in extremely small scale started to be studied using nanoporous materials such as silica gels (SGs), porous glasses (PGs), graphene oxide (GO), clay and metal organic frameworks (MOFs). While preliminary investigations focused on how gas hydrates behave in the porous environments found in geo-sediments, research has expanded to using enhanced properties of confined gas hydrate for new applications such as gas storage and separation. In addition, scientific curiosity about the science of gas hydrate at the nanoscale has been a great motivation for this new pioneering area. It is known that confinement in porous media changes the properties of gas hydrates such as cage occupancy [11], formation kinetics and thermodynamic behavior [12], of which the change in phase behavior is considered to be the most urgent issue to be investigated. This is because phase equilibrium studies have been providing the most fundamental and basic data in gas hydrate research on the conditions under which clathrate structures can form and dissociate.

In general, the phase equilibrium point in bulk gas hydrate is determined from the pressure (P) - temperature (T) trace curve obtained by recording the change of pressure during a cycle of the cooling and heating process at isochoric conditions. Specifically, a vessel containing water is pressurized with a target gas and kept closed at a temperature at which gas hydrate does not form, then goes through a slow cooling process until the end of hydrate formation, during which the formation of the gas hydrate can be checked by observing any rapid pressure drop. After the end of gas hydrate formation, the reactor is slowly heated toward the starting temperature. As gas hydrate formed during the cooling process dis-

†To whom correspondence should be addressed.
E-mail: hlee@kaist.ac.kr

sociates, the pressure of the reactor is recovered and the point at which the cooling and heating line meet is the phase equilibrium point of the gas hydrate. Different from the simple procedure for phase equilibrium point measurement in a bulk system, for nano-confined gas hydrates, a careful experimental procedure with accurate analysis of experimental results should be followed due to the complex phase behaviors of gas hydrates in nonporous materials with broad pore size distribution and interaction with the surface. For this reason, an exact understanding of both experimental methodology and scientific phenomena should be achieved.

In this review, we survey the previous studies on the phase behavior of gas hydrates in various nanoporous materials and related physical phenomena in the system. Moreover, we include and provide valuable information and knowledge that we have learned from our own experiences exploring the gas hydrate system at the nanoscale. In particular, we have included a chapter to introduce peculiar phenomena observed in our previous investigations that measured phase equilibria of gas hydrate in porous media with micropores (<2 nm), including MOFs, GO, and crystalline swelled clay. Contrary to the usual *P-T* trace curve of a bulk gas hydrate system in which the cooling and heating line meet after the temperature recovers to the starting point, the pressure of CO_2 is not recovered with the presence of micropores; water-filled micropores provide a favorable environment for hydrophilic gas molecules such as CO_2.

EXPERIMENTAL METHODOLOGY FOR GAS HYDRATE PHASE EQUILIBRIUM MEASUREMENT

1. Experimental Method for the Phase Equilibria of Gas Hydrates in Bulk State

In general, the phase equilibria line indicates the conditions under which multiple phases coexist at equilibrium. For gas hydrates, the phase equilibria line indicates the boundary pressure and temperature conditions at which gas hydrate structures can exist. This originates from the experimental method of determining the phase equilibrium point, comprising the subsequent cooling and heating procedure for the formation and dissociation of gas hydrates, respectively, as an isochoric process. While there have been a few

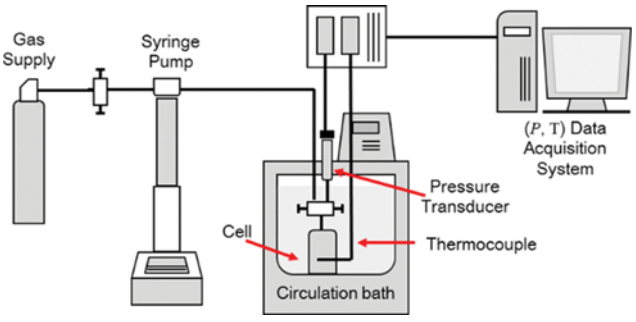

Fig. 1. Schematic description of experimental apparatus for phase equilibrium point measurement.

methods to determine the equilibrium point, including isobaric, isothermal and isochoric methods, the isochoric method has been the most widely used due to its simplicity and universal applicability to any kind of gas or water system. For this reason, we describe it in detail.

The experimental apparatus for isochoric measurement is composed of three parts as shown in Fig. 1: a high pressure gas injector, a high pressure stirring vessel equipped with a *P* transducer and a *T* thermocouple, and a data acquisition system. The high pressure vessel containing water is pressurized with gas at sufficient pressure and temperature so that the gas hydrate does not form (the right uppermost point in Fig. 2(a)). Stirring follows to generate a large interfacial area between the gas and water for the effluent gas diffusion into the water phase. Once pressure and temperature are stabilized the vessel experiences cooling, during which a rapid pressure drop is observed, indicating gas hydrate formation. The formation of solid gas hydrates may stop the stirring. The cooling is continues until no further pressure drop is observed. Then the vessel is heated slowly toward the starting temperature. During the heating procedure, the heating rate should be low enough to guarantee an equilibrium state over the entire heating procedure: 0.1 K/h is generally accepted in a lab-scale vessel. For heating, there are two methods to increase temperature: continuous heating and multi-step heating. In the former, the temperature is continuously changed, but the latter involves stepwise heating with waiting for the tem-

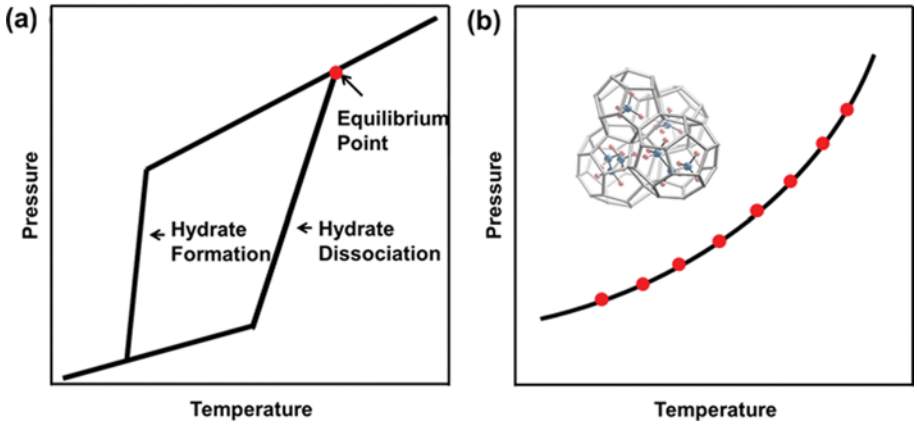

Fig. 2. (a) Pressure - temperature trace curve of gas hydrates in a bulk state. (b) Phase equilibrium curve of gas hydrates. Red dots indicate phase equilibrium points.

perature to arrive at an equilibrium state after the temperature is increased. While Uchida et al. found a consistency of the results from these two methods by showing that the same phase equilibrium data of gas hydrates confined in glass media were obtained from both methods within an experimental error range [13], Tohidi et al. revealed that the continuous heating method did not provide precise data and reproducibility due to insufficient time for the system to reach equilibrium [14]. Considering these controversial results, the more conservative method is recommended for phase equilibrium measurement, which is the multistep heating method.

Different from the rapid pressure drop during formation, the dissociation of gas hydrates is conducted over a broad temperature range, during which the pressure in the vessel is recovered. As a result of the cycle, a *P-T* trace curve is obtained as shown in the Fig. 2(a), in which the point at which the cooling and heating line meet is the equilibrium point of the gas hydrate. The equilibrium points comprise a phase equilibria line, and gas hydrates are stable at the condition above the line in Fig. 2(b).

While the phase equilibrium point of bulk gas hydrate is simply determined, that of gas hydrates formed in nanoporous space requires a more complex and precise procedure for the determination of the equilibrium point on the heating line due to the influence of pore size distribution and surface interaction.

2. Experimental Method for the Phase Equilibria of Gas Hydrates in Meso/Macroporous Materials

The measurement of phase equilibrium point of gas hydrates confined in nanoporous media is performed with the same method as with the bulk state except water-saturated porous materials are used instead of bulk liquid water. Prior to measuring the P-T trace curve to determine the equilibrium point, nanoporous materials including water should be prepared. At this stage, it is important to saturate the pores of the nanoporous materials with water without either containing excess bulk water phase outside of porous materials or the nanopores remaining partially filled. The former causes the appearance of bulk and confined gas hydrate phases together during measurement and interferes with analyzing the confined gas hydrate phase only. The latter makes it impossible to find the relation between pore size and the properties of confined gas hydrates.

There are two experimental methods to make water-filled porous materials as shown in Fig. 3. One is applying sonication after adding water and porous materials in a bottle for a long time (about 1 day) [15], and the other is the vacuum evaporation method [16]. While both methods are available, the former provides much faster water saturation, and the latter is more widely applicable to saturate nanoporous materials with water regardless of the types of nanoporous materials, for which water condensation in 100% relatively humid condition was used. In detail, nanoporous materials are kept in 100% relative humidity in a closed system, such as a desiccator, in which water molecules in the air condense in the pores gradually and fill the pores. Since this procedure requires a long time, a vacuum-assisted procedure is adopted as follows. Nanoporous materials and slightly more than the amount of water equivalent to the volume of the nanopores are placed in a vacuum oven and the inside is rapidly evacuated and closed. After evacuation, the inside of the oven becomes highly humid and faster water condensation in energetically favored pores is achieved. The water saturation of nanoporous material can be checked by comparing the mass change before and after the procedure; if water saturation is achieved, the weight of the material should increase as much as the pore volume of the porous material.

Different from the procedure for bulk liquid, stirring inside of the high pressure vessel is not essential for a porous system, because nanoporous materials usually have a form of solid particles, and pores between particles provide a higher contact interface for the transport of gas into the confined water than liquid water. However, the time for equilibrium could be longer than for the bulk state because the diffusion of gas into water-filled nanopores may require more time. The appropriate heating rate for equilibrium can be confirmed by measuring the time required for the pressure to be stabilized after the changing temperature. For example, if pressure is stabilized in 30 min after changing the temperature 0.1 K, a stepwise heating rate lower than 0.2 K/h should be adopted. The most pronounced difference for nanoporous material is in the determination of the phase equilibrium point on the dissociation line of the *P-T* trace curve. While the shape of the dissociation curve is not considered for the equilibrium point determination of bulk hydrate, it is the most important data for the gas hydrates formed in nanoporous materials, because pore characteristics such as pore size distribution are reflected on it.

PHASE EQUILIBRIA BEHAVIOR OF GAS HYDRATES IN MESO/MACROPOROUS MATERIALS

1. Phase Equilibria of Gas Hydrates in Nanoporous Silica Gel

For the phase equilibria study of gas hydrates in nanoporous materials, nanoporous SGs and PGs have been used the most frequently. SGs with unimodal pore size distribution provide much

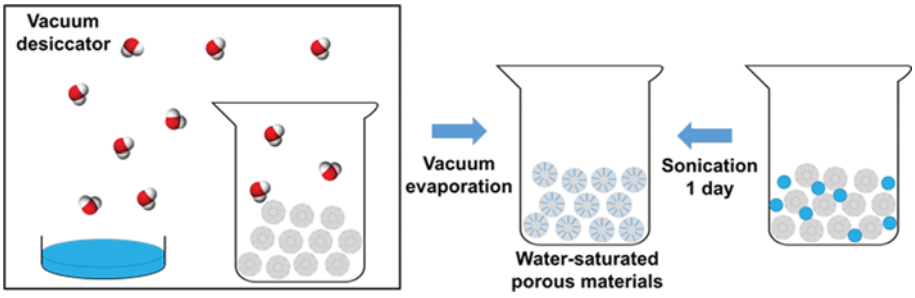

Fig. 3. Experimental methods to prepare water-saturated porous materials.

easier linkage between the pore size and equilibrium point of confined gas hydrate than other porous materials with complicated pore size distribution. To the best of our knowledge, Handa and Stupin were the first to study the thermodynamic properties and phase equilibria of gas hydrates in nanoporous material by exploring phase behaviors of CH_4 and C_3H_8 hydrates in SG with a 15 nm mean pore diameter in 1992 [16]. They were motivated by a discrepancy between the thermodynamic properties of lab-synthesized gas hydrates and natural gas hydrates buried in sediment. This is because sediment particles and their geometrical constraints cause a confinement effect such as capillary pressure on the confined gas hydrates. They reported a considerably inhibited phase different from the bulk phase which was due to the reduced activity of the confined water.

Uchida et al. also reported a shift of CH_4, CO_2 and C_3H_8 hydrate phase equilibria in PGs with pore diameters ranging from 4 to 100 nm toward left in *P-T* diagram, which was different in the bulk state (so called inhibition) [17]. By applying the Gibbs-Thomson effect for the analysis of the observed inhibition, they revealed the effect of reduced water activity on the inhibition of the equilibrium point. Moreover, they provided a mathematical explanation of the relation between pore size and phase equilibrium data; the equation was written as

$$\frac{\Delta T}{T_d} = -4\gamma_{HW}(\rho_H L_H d)^{-1}$$

where γ_{HW} represents hydrate-water interfacial free energy, ρ_H is the density of methane hydrates, L_H is the latent heat of the dissociation of pore hydrates, d is the pore diameter, and ΔT: T_d-T_e, T_e and T_d are the dissociation temperatures of methane hydrates in the bulk phase and in confined small pores, respectively. As represented in the equation, the shift of phase equilibrium is a function of the reciprocal pore diameter, which trend was also observed in the results from other groups. Based on experimental data and investigation, the Smith group conducted thermodynamic modeling to understand and predict the thermodynamic properties and phase equilibria of gas hydrates in porous SG [18-21]. The Smith group has developed a model to relate thermodynamic properties, such as fugacity and enthalpy, with pore size based on statistical thermodynamics as well as experimental equilibrium data of ethane and propane hydrates in porous media. Klauda and Sandler also suggested a model to predict hydrate phase behaviors in porous media, which considered the effects of surface energy and pore size distribution [22]. In addition Seo et al. measured phase equilibria of CH_4 and CO_2 hydrates in silica gel with 6.0, 15.0 and 30 nm of nominal pore diameters and compared to the calculated results based on van der Waals-Platteeuw model [23]. Importantly, they have incorporated a correction term into the model to account for both capillary effect and water activity decrease induced by geometric constraints, which provided enhanced accuracy in the prediction of phase equilibria of gas hydrates in nanoporous SG.

Nevertheless, exact correlation between pore size and equilibrium point was not achieved at that time. This was because porous materials had broad pore size distribution and gas hydrates dissociated in a broad temperature and pressure range, which made it hard to find the exact pore size and corresponding dissociation point. For example, the dissociation point of gas hydrates measured in SG with 15 nm of nominal pore dimeter did not correspond to a 15 nm pore, which point originated from the one of a pore diameter within the pore size distribution. For this reason, an exact model that analyzed gas hydrate dissociation behavior in porous media considering pore size distribution is of great importance.

In response to these circumstances, Anderson et al. provided a more accurate conceptual model to analyze experimental results (the dissociation line), by which experimentally measured phase equilibrium data can be interpreted in association with the mean pore diameter [24,25]. The model is based on the idea that gas hydrates in smaller pores dissociate earlier during the heating process of isochoric equilibrium measurement. Accordingly, a *P-T* point where the gas hydrate starts to dissociate corresponds to the equilibrium point of gas hydrates in the smallest pore in porous media, and the *P-T* point where dissociation finishes corresponds to the equilibrium point in the largest pore. More importantly, the point of slope inflection corresponds to the equilibrium point of gas hydrates in the mean pore diameter when the porous materials have a Gaussian-like pore size distribution (see Fig. 4). Since general porous SGs have Gaussian-like pore size distribution, the model provides a method to determine the exact phase equilibria point of gas hydrates in a mean pore diameter, which can be determined by finding the temperature at which the differentiate of the dissociation curve by T equals zero (dP/dT=0) and the corresponding pressure.

Based on that model, a few studies measured the exact phase equilibria of gas hydrates in SG pores. Kang et al. measured CO_2 and CH_4 hydrate equilibria in SGs with 6, 30 and 100 nm or pore diameter [26]. Interestingly, they revealed that there was a stronger inhibition on confined gas hydrates in the smaller pores, but the structure and cage occupancy of methane hydrate in SG was the same as that of the bulk state regardless of pore size. Seo et al. [27] also investigated the ethane and propane hydrates in SGs with 6, 15, 30 and 100 nm pore diameters for the purpose of examining the potential of hydrate formation in SG for natural gas storage and transport. Both experimental results showed good agreement with the prediction using a modified van der Waals-Plat-

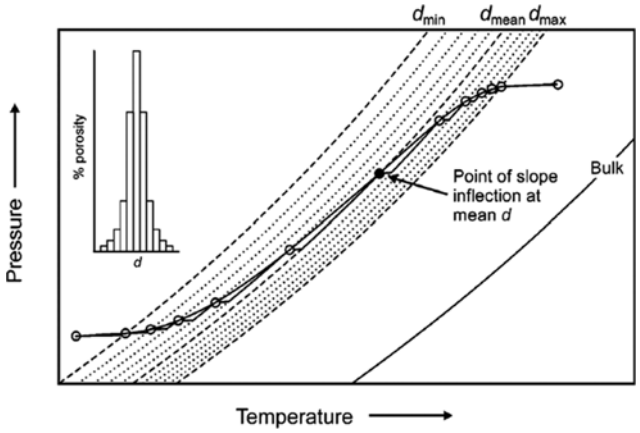

Fig. 4. Theoretical equilibrium dissociation path for a porous medium with multiple pore diameters (pore size distribution shown in inset). Reprinted with permission from ref. 24. Copyright (2015) American Chemical Society.

teeuw equation. State-of-the-art thermodynamic modeling for the phase equilibria of gas hydrates in porous media has been well introduced in the report of Seo [27].

The previous phase equilibria data of pure CO_2, CH_4, C_2H_6 and C_3H_8 in nanoporous materials are summarized in the following table with respect to mean pore diameter.

2. Factors Influencing Phase Equilibria of Confined Gas Hydrates

Activity of water in confined pores has been considered to be the main driving force to determine the phase equilibrium behaviors of confined gas hydrates, which means that consideration on the factors that influence water activity is essential. Capillary effect originating from geometrical constraints is crucial for the reduction of water activity, which can be expressed as [27]

$$\ln a_W = \ln(x_W \gamma_W) - \frac{F V_L \cos\theta \sigma_{HW}}{rRT}$$

where F is the shape factor reflecting curvature of the hydrate-liquid interface, V_L is the molar volume of pure water, θ is the wetting angle between pure water and hydrate phases, σ_{HW} the interfacial tension between hydrate and liquid water phases, r is the pore radius. This equation indicates that the shape, size and surface characteristic of pore are important factor influencing the phase equilibria of confined gas hydrate phase.

3. Phase Equilibria of Gas Hydrates in Nanoporous Silica Gel with the Presence of Electrolytes

The phase equilibrium of gas hydrates in porous media was also measured with the addition of electrolytes to predict the phase behavior in actual sediment systems where sea water was included in the pores of sediments. The studies regarding the influence of electrolytes on phase equilibria of gas hydrates in SG have been predominantly performed by Seo and coworkers. Seo et al. measured the phase equilibria for the ternary CH_4+NaCl+water and CO_2+NaCl+water mixtures in 15.0 nm SG pores and for the ternary CH_4+CO_2+water mixtures with 20, 40, 60, 80 mol% of CO_2 vapor compositions in 6.0, 15.0, and 30.0 nm of SG pore [15]. Seo et al. measured phase equilibria for C_2H_6, and C_3H_8 hydrates with NaCl in SG with nominal pore diameter of 6.0 (3 wt%), 15.0 (3 wt%), and 30.0 nm (3, 10 wt%) [28]. Also, they measured hydrate phase equilibria for the ternary CH_4 (90%)+C_3H_8 (10%)+water mixtures and for the quaternary CH_4 (90%)+C_3H_8 (10%)+NaCl+water mixtures of two different NaCl concentrations (3 and 10 wt%) in SG pores with pore diameters ranging from 6.0 to 100.0 nm [29]. Moreover, Seo et al. measured phase equilibria for the quaternary CH_4 (90%)+C_2H_6 (7%)+C_3H_8 (3%)+water mixtures in silica gel pores of nominal diameters of 6.0, 15.0, and 30.0 nm and for the quinary CH_4 (90%)+C_2H_6 (7%)+C_3H_8 (3%)+NaCl+water mixtures of two different NaCl concentrations (3 and 10 wt%) in SG with pore diameters of 30.0 nm along with the characterization on structure, cage occupancies of guests and hydration number of the formed gas hydrate phase by 13C NMR [30]. The presence of large C_3H_8 molecules makes sII structure to be formed, wherein small cages are occupied by CH_4 and large cages by CH_4, C_2H_6, and C_3H_8 molecules.

Seo et al. provided important information for the understanding of gas hydrate phase behaviors in SG with presence of electrolytes: 1) Smaller pore size and higher electrolyte concentration cause stronger reduction of water activity and the gas hydrate phase revealing more highly inhibited phase behaviors, and 2) Electrolytes and geometrical constraint hardly change the structure of gas hydrates formed in SG pores.

4. Phase Equilibria of Gas Hydrates in Nanoporous Materials and Application for CO_2 Capture

Seo et al. paved the way to extend gas hydrate research in nanoporous materials to the application for CO_2 separation/capture study [31]. They provided hydrate phase equilibria for ternary N_2+CO_2+water mixtures in 30 nm of SG using gas mixtures containing different compositions of CO_2 (10.0, 17.0, 35.0, and 50.0 mol%). Based on the equilibrium data, the enrichment of CO_2 from 10 to 96% was demonstrated through three times of successive formation and dissociation of gas hydrate in 30 nm of SG (See Fig. 5). In addi-

Table 1. Phase equilibrium data of CO_2 hydrate in porous materials

6 nm (SG)[26]		6 nm (SG)[23]		9.2 nm (PG)[25]		15 nm (SG)[23]		15.8 nm (PG)[25]	
T (K)	P (Mpa)	T (K)	P (Mpa)	T (K)	P (Mpa)	T (K)	P (Mpa)	T (K)	P (Mpa)
269.88	1.4	274.3	2.215	272.6	1.931	272.3	1.447	273	1.613
271.12	1.69	275.3	2.664	274.7	2.544	274.25	1.865	275.7	2.261
273.78	2.56	276.15	3.072	270.2	1.448	275.65	2.283	277.9	3.068
275.87	3.48	276.71	3.44			276.93	2.662	278.2	3.172
276.52	3.83	277.65	3.89			278.34	3.216		
		278.98	3.598			280.45	3.4		
		279.7	3.918			281.35	3.88		

20 nm (SG)[26]		30 nm (SG)[23]		30.6 nm (PG)[25]		100 nm (SG)[26]	
T (K)	P (Mpa)	T (K)	P (Mpa)	T (K)	P (Mpa)	T (K)	P (Mpa)
272	1.29	271.8	1.13	273.1	1.407	271.25	1.06
275.15	1.78	273.65	1.433	277.9	2.579	276.15	1.82
279.35	3.25	276.05	1.95	279.8	3.33	279.65	2.92
280.15	3.65	277.95	2.418			281.65	3.93
		279.25	2.913				

Table 2. Phase equilibrium data of CH_4 hydrate in porous materials

4 nm (PG)[47]		6 nm (SG)[26]		6 nm (SG)[47]		6 nm (SG)[23]		9.2 nm (PG)[25]	
T (K)	P (Mpa)	T (K)	P (Mpa)	T (K)	P (Mpa)	T (K)	P (Mpa)	T (K)	P (Mpa)
273.1	8.8	269.65	2.84	278.3	9.03	275.3	5.17	271.8	3.689
		271.45	3.82	278.6	9.86	276.65	6.19	278.6	7.55
		273.75	5.46			277.95	7.2	283.1	12.5
		276.15	7.45			279.35	8.275		
		278.58	9.94			279.95	9.326		
						280.95	10.5		

10 nm (PG)[47]		14 nm (SG)[16]		15 nm (SG)[47]		15.8 nm (SG)[25]		30 nm (PG)[17]	
T (K)	P (Mpa)	T (K)	P (Mpa)	T (K)	P (Mpa)	T (K)	P (Mpa)	T (K)	P (Mpa)
277.2	6.5	263	2.603	277.15	4.825	277.8	5.564	278.2	5
277.6	6.6	264.2	2.691	279.15	6.06	276.9	5.019	279.5	5.9
277.7	7.1	264.6	2.738	280.45	7.16	282.9	9.66	279.7	5.6
		266.2	2.908	281.75	8.243	285.6	13.307	280.6	7
		268.2	3.188	282.88	9.275			281.7	6.8
		270	3.551	283.7	10.285			281.7	7.4
		272	4.011					283.7	8.5
		273.2	4.347						
		274.2	4.61						
		276.2	5.186						

30 nm (SG)[26]		30 nm (PG)[47]		30 nm (SG)[23]		30.6 nm (PG)[25]		50 nm (SG)[17]	
T (K)	P (Mpa)	T (K)	P (Mpa)	T (K)	P (Mpa)	T (K)	P (Mpa)	T (K)	P (Mpa)
270.9	2.38	259.7	1.65	276.33	4.012	280.5	6.405	278.5	4.8
275.15	3.67	260.5	1.74	278.3	4.948	283.8	9.17	281.3	6.4
278.15	5.11	264.8	1.89	280.55	6.175	287.5	14.065	281.5	6.6
280.25	6.4	265.6	2.04	282.15	7.3			281.6	6.7
283.2	8.73	267.3	2.16	283.33	8.285				
		269	2.08	284.53	9.638				
		270	2.22						
		270.8	2.38						
		273.2	2.99						
		273.6	3.11						
		274.2	3.24						
		274.8	3.42						
		277.5	4.59						
		278.1	4.92						
		278.2	5.02						
		279.6	5.87						
		279.7	5.59						
		280.6	7						
		281.7	6.83						
		281.7	7.38						
		283.7	8.5						

50 nm (SG)[47]		100 nm (PG)[47]		100 nm (SG)[26]	
T (K)	P (Mpa)	T (K)	P (Mpa)	T (K)	P (Mpa)
278.7	4.8	274.2	2.95	272.55	2.47
281.3	6.42	274.2	3.01	276.2	3.62
281.5	6.61	275.6	3.41	278.35	4.5
281.6	6.68	277.6	4.12	280.85	5.84
		279.5	5.02	284.25	8.32
		281	5.72		

tion they demonstrated a fast formation rate and high conversion yield of gas hydrates in SG without stirring. Their preliminary result showed the potential of combining gas hydrate technology with SG for eco-friendly and efficient CO_2 separation. For the application of gas hydrate technology in precombustion CO_2 separation, hydrate phase equilibria for the H_2 (60%)+CO_2 (40%)+water mixtures in SG with 6, 15, 30, 100 nm mean pore diameters measured by Park et al. [32].

Gas hydrate formation in nanopores accompanies inhibition of the phase equilibria line, which makes it harder to achieve conditions required for the CO_2 capture using gas hydrates in porous materials. For this reason, promoter molecules were added to make the

Table 3. Phase equilibrium data of C_2H_6 hydrate in porous materials

6 nm (SG)[20]		6 nm (SG)[27]		10 nm (SG)[20]		15 nm (SG)[20]		15 nm (SG)[27]	
T (K)	P (Mpa)	T (K)	P (Mpa)	T (K)	P (Mpa)	T (K)	P (Mpa)	T (K)	P (Mpa)
246.15	0.137	271.97	0.975	243.15	0.112	245.15	0.125	274.73	0.976
247.15	0.154	274.48	1.42	251.15	0.183	246.15	0.131	277.6	1.367
248.15	0.145	275.55	1.733	252.15	0.191	247.15	0.143	279.99	1.895
249.15	0.158	276.99	2.11	253.15	0.201	248.15	0.15	280.94	2.244
250.15	0.17	278.07	2.529	259.15	0.253	249.15	0.16	282.54	2.814
251.15	0.179			260.15	0.272	250.15	0.17		
252.15	0.187			261.15	0.284	251.15	0.179		
253.15	0.205			262.15	0.298	252.15	0.186		
253.15	0.205			263.15	0.311	253.15	0.196		
254.15	0.222			264.15	0.324	254.15	0.207		
255.15	0.245			265.15	0.353	255.15	0.217		
256.15	0.269			266.15	0.396	256.15	0.227		
257.15	0.29			267.15	0.44	257.15	0.239		
258.15	0.316			268.15	0.489	262.15	0.28		
259.15	0.345			269.15	0.53	263.15	0.305		
260.15	0.379			271.15	0.675	264.15	0.324		
261.15	0.415			272.15	0.754	265.15	0.34		
262.15	0.452			273.15	0.827	266.15	0.376		
263.15	0.493			274.15	0.926	267.15	0.419		
264.15	0.534			275.15	1.025	268.15	0.466		
265.15	0.582			276.15	1.136	269.15	0.516		
266.15	0.634			277.15	1.255	271.15	0.633		
267.15	0.677					272.15	0.702		
268.15	0.755					237.15	0.773		
269.15	0.821					274.15	0.864		
271.15	0.968					275.15	0.961		
272.15	1.049					276.15	1.044		
273.15	1.142					277.15	1.121		
274.15	1.236								
275.15	1.33								
276.15	1.423								
277.15	1.504								

30 nm (SG)[27]		100 nm (SG)[27]	
T (K)	P (Mpa)	T (K)	P (Mpa)
277.2	0.903	278.69	1.024
280.1	1.301	281.1	1.414
281.84	1.663	283.15	1.863
283.61	2.157	284.13	2.162
284.4	2.505	285.24	2.556

gas hydrate form at much milder conditions. Park et al. also measured hydrate phase equilibria of H_2 (60%)+CO_2 (40%)+water with the presence of tetrahydrofuran (promoter molecule) with varying concentration from 1 to 10 mol% [32]. Kang et al. provided hydrate phase equilibria for H_2+CO_2+tetrabutyl ammonium bromide+water system for the utilization in precombustion capture [33].

The history of hydrate-based CO_2 capture technology and its state-of-the-art can be read in the reviews from other groups [34-36].

GAS HYDRATES IN SUB-NANOMETER SCALE: MICROPOROUS MATERIALS

The pores in the size of a meso/macroporous region provide us with enough space for the inclusion of more than two lattices of gas hydrate, which has been the basic and fundamental starting point where gas hydrate research in a confining nanospace began. In the study of peculiar phenomena of gas hydrates in nanoporous materials, an interesting question is arose, which is about the gas

Table 4. Phase equilibrium data of C_3H_8 hydrate in porous materials

4 nm (SG)[18]		6 nm (SG)[18]		6 nm (SG)[15]		10 nm (SG)[15]		14 nm (SG)[16]	
T (K)	P (Mpa)	T (K)	P (Mpa)	T (K)	P (Mpa)	T (K)	P (Mpa)	T (K)	P (Mpa)
246	0.19	253	0.16	263.53	0.233	263	0.201	253	0.777
246.5	0.194	254	0.165	264.22	0.265	263.5	0.208	261.2	1.391
247	0.197	255	0.171	264.84	0.321	264	0.215	261.2	1.451
247.5	0.202	256	0.175	264.86	0.309	264.5	0.221	262.2	1.487
248	0.205	257	0.181			265	0.231	262.6	1.541
248.5	0.208	258	0.186			265.5	0.234	263.2	1.599
249	0.212	259	0.196			266	0.241	263.6	1.632
249.5	0.217	260	0.204			266.5	0.25	264.2	1.7
250	0.22	261	0.215			267	0.26	264.6	1.76
250.5	0.224	262	0.226			267.5	0.27	265.2	1.846
251	0.228	263	0.238			268	0.283	265.6	1.927
251.5	0.232	264	0.251			268.5	0.294	266	2.003
252	0.237	265	0.264			269	0.306	266.6	2.105
252.5	0.24	266	0.273			269.5	0.319	267.2	2.207
253	0.244	267	0.28					267.6	2.309
253.5	0.25	268	0.287					268.2	2.44
254	0.255							268.8	2.601
254.5	0.26							269.6	2.8
255	0.265							270	2.964
255.5	0.27							270.8	3.15
256	0.275							270.8	3.212
256.5	0.279							271.2	3.336
								271.8	3.522
								272	3.653

15 nm (SG)[18]			15 nm (SG)[15]		30 nm (SG)[15]		100 nm (SG)[15]	
T (K)	P (Mpa)	(Mpa)[b]	T (K)	P (Mpa)	T (K)	P (Mpa)	T (K)	P (Mpa)
264.2	0.175	0.181	268.48	0.187	271.94	0.176	272.83	0.192
265.2	0.185	0.191	269.95	0.251	273.12	0.233	274.3	0.259
265.6	0.195	0.196	270.47	0.286	273.98	0.286	275.32	0.325
266	0.196	0.2	271.75	0.349	274.88	0.353	276.44	0.413
266.6	0.208	0.208	272.58	0.401	275.74	0.417	276.81	0.449
267.2	0.215	0.217						
267.6	0.226	0.226						
268.2	0.237	0.238						
268.8	0.252	0.253						
269.6	0.273	0.27						
270	0.278	0.279						
270.8	0.303	0.302						
271.2	0.326	0.315						

[a,b]Represent different types of SG

hydrates in a much smaller space, namely, micropores. The size of meso/macropores is different from the size of micropores (<2 nm). The micropore can afford to include either zero or only one lattice in terms of size. To explain and provide clues for understanding on the sub-nanometer scale, Lee and coworkers agonized over how to investigate the behaviors of gas hydrates as well as binary gas + water systems in a microporous region. They paid attention to microporous materials such as GO, clay, MOFs and SGs as useful tools to investigate the science at such an extremely small scale. By using the materials, they investigated the formation of gas hydrates in microporous materials through structural detection using XRD along with phase equilibria measurement.

MOFs are highly porous crystalline materials. A consecutive alternating connection of metal/metal oxide clusters and organic molecules *via* ligand bonding makes highly ordered and coordinated structures [37]. The pore size of MOF can be tailored by us-

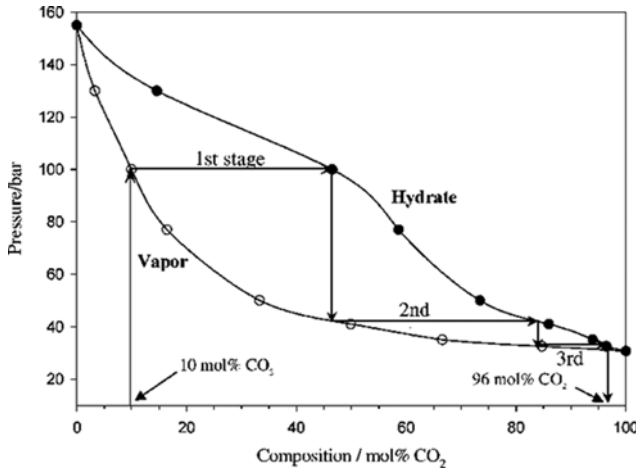

Fig. 5. Pressure-composition diagram of the ternary N_2+CO_2+water system measured at 272.1 K. The arrow traces conceptually the three-stage recovery process of CO_2 from a binary gas mixture. Reprinted with permission from ref. 31. Copyright (2015) American Chemical Society.

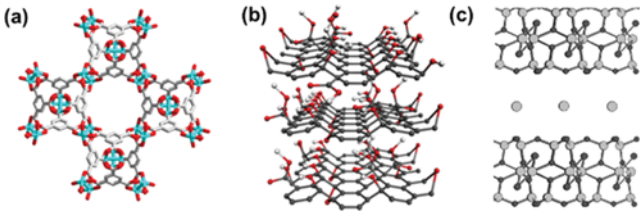

Fig. 6. Schematic description of microporous materials. (a) HKUST-1 metal organic framework, (b) graphene oxide and (c) montmorillonite.

ing organic molecules with various lengths and the intrinsic pores can include various molecules.

Lee et al. chose and used HKUST-1 MOF for the investigation of gas hydrates in MOFs [38], because of well-defined pore characteristics as well as high water stability [39]. The structure described in Fig. 6(a) represents HKUST-1, one of the most well-known MOF structures. While the pores of MOF have been filled with water and pressurized with CO_2 and CH_4 gases with a strong driving force (higher pressure and lower temperature than equilibrium line of bulk hydrate) to form gas hydrates, no formation of a confined gas hydrate structure in the micropore has been detected, indicating that the pores of MOF smaller than 1 nm do not provide a favorable environment for gas hydrate formation. Instead, a peculiar gas storage phenomenon has been observed in water-filled pores of MOF. They revealed that a considerable amount of CO_2 can be stored in the water-filled HKUST-1 micropore as a function of pressure without gas hydrate formation, but that of N_2 and H_2 has been negligible as seen in Fig. 7. To elucidate the origin of the abnormal gas storage phenomenon, the authors used molecular dynamic simulation, which revealed that the water-filled micropores of HKUST-1 provide a thermodynamically and kinetically favorable environment for CO_2 capture, but not for N_2 and H_2 capture. In addition the sites where CO_2 molecules exist were widened as higher pressure was applied: The interface between the MOF

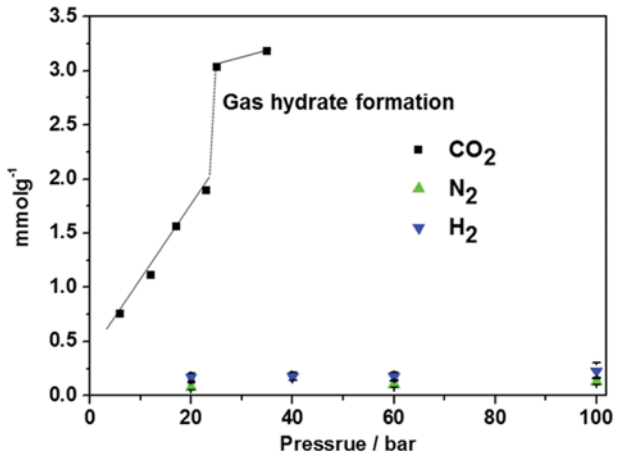

Fig. 7. Gas storage of WS-HKUST-1 at the indicated pressure at room temperature then kept at −30 °C. Reprinted with permission from ref. 38, copyright 2015 WILEY-VCH Verlag GmbH & Co. KGaA, Weinheim.

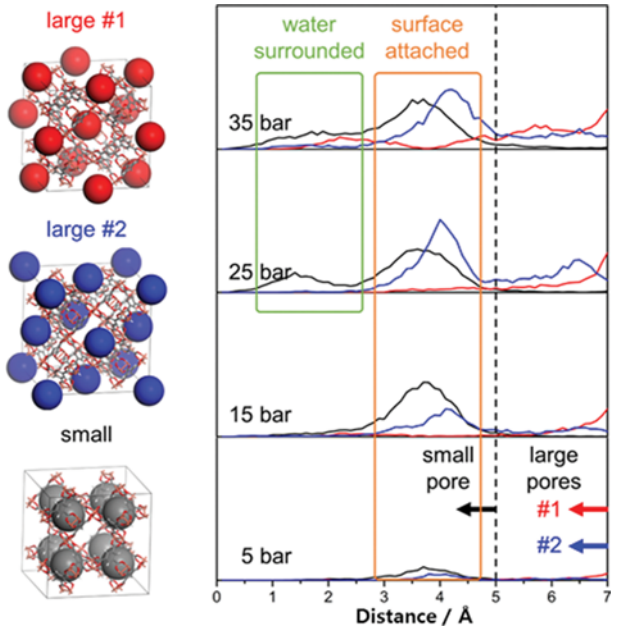

Fig. 8. Molecular dynamic simulation of CO_2 storage in water-filled pores of HKUST-1. Reprinted with permission from ref. 38, copyright 2015 WILEY-VCH Verlag GmbH & Co. KGaA, Weinheim.

wall and confined water molecules was the main storage site at low pressure (~15 bar), but CO_2 started to be included inside of confined water molecules at higher pressure, reminding a small gas hydrate cage that includes one gas molecule (Fig. 8). Moreover, the difference in the gas storage amount between CO_2 and N_2/H_2 has led to the separation of CO_2/N_2 and CO_2/H_2 gases, known as post/pre-combustion gases.

GOs are composed of the stacking of two-dimensional carbon layers on which hydrophilic functional groups such as epoxide, hydroxide and carboxylic acid are attached (see Fig. 6(b)). Stacking of the two-dimensional sheets makes a unique space between

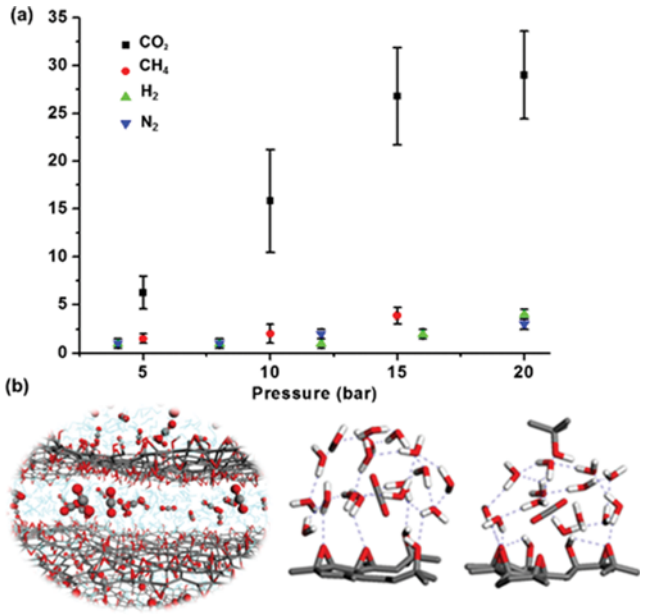

Fig. 9. (a) Gas storage amount of various gas molecules about the injected gas pressure at 15 °C. After pressurizing the gases at room temperature, all samples were cooled to −30 °C. (b) Representative local cage like structure surrounding CO_2. Hydrogen bonding network is shown with dashed line. Reprinted with permission from ref. 41. Copyright 2015 American Chemical Society.

neighboring layers, the so-called interlayer space, with strong hydrophilicity. As the interlayer absorbs water, interlayer space increases from ~0.6 nm to ~1.2 nm [40]. Lee et al. observed the interesting gas storage behavior of confined water in water-filled interlayer of GO [41]. The water-filled interlayer had a higher CO_2 storage amount than CH_4, H_2 and N_2 gases (see Fig. 9(a)). A molecular dynamic simulation revealed that CO_2 molecules in the swollen GO had a greater chance to form a stable binding structure with the surrounding water molecules due to the hindered dynamics of water molecules in the confining interlayer. CO_2 molecules were mainly located in the middle of the interlayer, mostly surrounded by 13 water molecules and 5 O atoms from the GO surface, by which form a cage-like structure consisting of hydrogen bonding networks as seen in Fig. 9(b). While the exact gas hydrate structure was not formed in the system, this result showed the effect of a small confining environment on the properties of water and its gas storage properties. It is noteworthy that confined gas hydrates formed in the nanopores, including the intergranular and interparticle space of MOF and GO, which revealed inhibited phase behavior due to the confining-induced capillary effect and surface interaction [42,43]. Phase equilibria of gas hydrates are more strongly shifted toward an inhibited region than other porous materials due to a severe reduction of water activity on the hydrophilic surface GO. This result indicated the importance of surface characteristics on the properties of confined gas hydrates.

The issue discussed in this section, the possibility of gas hydrate formation in the microporous region, can be extended to questions about the natural gas hydrates in sediment because sediment components also possess micropores. Among sediment components, montmorillonite is one of the representative geochemical components that possesses a pore structure similar to that of GO, which can cause a confining effect on the gas-water system and change the properties of the confined gas hydrates. The interlayer spacing of clay changed according to the amount of water fraction from 0.95 nm to infinite dispersion [44], which provided us an opportunity to observe the formation of gas hydrate in relation to the size of the confining space. Guggenheim et al. suggested that methane hydrate structures can be stably formed in interlayers when the interlayer distance is 2.2 nm (a size that includes a lattice of methane hydrate) [45]. However, no gas hydrate structure formed when the interlayer space was 1.59 nm at a crystalline swollen state due to the size of the interlayer (~0.6 nm) being smaller than that of a small 5^{12} cage of gas hydrate (~0.8 nm) as described in Fig. 10 [46]. Instead of gas hydrate formation, an unusual CO_2 dissolution in intercalated water was observed during phase equilibrium measurement. The dissolved CO_2 in the water-filled interlayer was kinetically and thermodynamically stable even at a temperature as high as 50 °C under gas pressure.

Unusual CO_2 dissolution (storage) in water-filled microporous materials was observed in various microporous materials such as

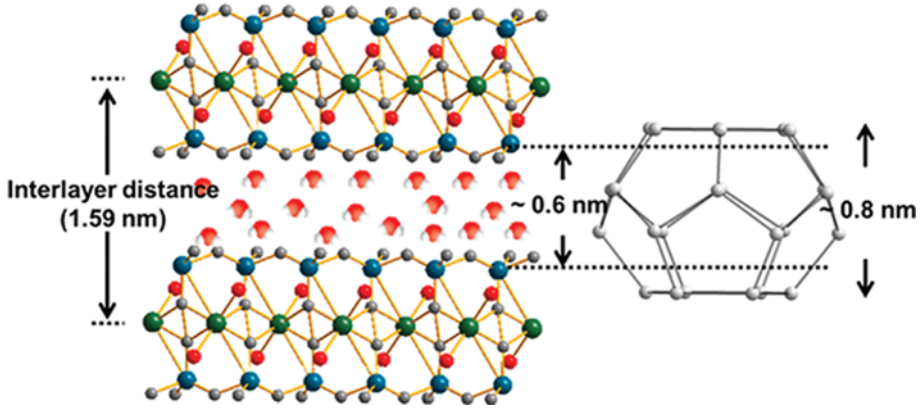

Fig. 10. Schematic illustration of Na-montmorillonite and 5^{12} cage of sI hydrate, respectively. The projection of clay is along the b axis. Reprinted with permission from ref. 46. Copyright 2015 American Chemical Society.

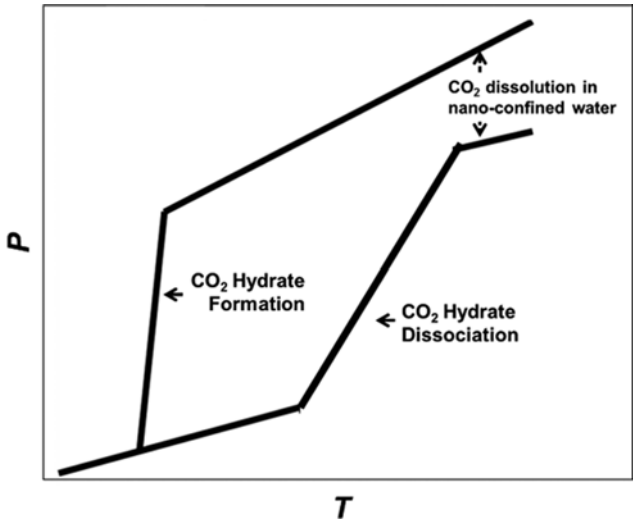

Fig. 11. *P-T* trace curve of CO_2 hydrates in the presence of microporous materials.

MIL-53 (Matériaux de l'Institut Lavoisier -53) MOF, montmorillonite and GO [42,43,46], which was reflected by the appearance of a CO_2 pressure gap on the *P-T* trace curve during the measurement of the phase equilibria point (see Fig. 11). A pressure-gap due to the lack of recovery of pressure appeared in the *P-T* trace curve of the CO_2 gas hydrate, but not in CH_4 hydrate with a larger pressure-gap at a higher starting pressure. Considering that all microporous materials have different pore shapes and properties, GO (hydrophilic surface, slit pore), MIL-53 (surface covered with metal oxide and benzene ring, spherical pore), montmorillonite (negative electrostatic surface, slit pore), the shape and surface properties of the material does not seem to be a major factor in the appearance of pressure gap; rather, the size of the pore is more important. This is further confirmed from the result of control experiments by Lee et al, wherein GO without interlayers showed no CO_2 pressure gap [40] and SG with a pore size less than 2 nm had an unusual CO_2 pressure gap [43], which means that the sub-nanometer space is the origin of the peculiar phenomena.

As reviewed in this section, Lee's group tried to uncover the peculiar gas storing phenomenon and examine the possibility for gas hydrate formation in microporous materials including Na-montmorillonite, GO, MOFs and SGs. As a result, valuable information to understand this phenomenon was provided. The results can be summarized as follows: 1) Strong CO_2 dissolution appears mainly in pores of less than ~2 nm instead of gas hydrate formation; 2) Higher gas storage amount at higher *P* and lower *T* conditions; 3) Storage of CO_2 in both thermodynamically and kinetically stable states; and 4) Extension of these phenomena for other hydrophilic gases. These results provide not only basic knowledge that will be helpful for analyzing gas hydrate formed in nanoporous materials, but also give hints to understanding the behavior of gas molecules in a few nanometer-space filled with water.

CONCLUSION

To understand the appearance of gas hydrates in sediments and the potential application of gas hydrate technology for CO_2 capture, there has been increasing interest in the phase behaviors of gas hydrates in porous media. To provide a precise analysis of the phase equilibria, experimental procedures, determination of equilibrium point and thermodynamic modeling should be adopted appropriately. In this review we have provided a method to prepare water saturated porous materials, to measure *P-T* trace curves, for determining the equilibrium point from the dissociation line of porous materials. The phase behaviors of gas hydrates show a tendency: a higher inhibition with a smaller pore size due to the capillary-induced reduction of water activity.

As the pore size decreased to 2 nm (microporous region), peculiar gas storing phenomena were realized instead of gas hydrate formation. The water-filled small pore revealed a noticeable storage capacity for CO_2 gas. The CO_2 storage features imply potential for CO_2 separation and storage.

ACKNOWLEDGEMENT

This research was supported by Basic Science Research Program through the National Research Foundation of Korea (NRF) funded by the Ministry of Education (2015R1A6A3A01060008).

NOMENCLATURE

γ_{HW} : hydrate-water interfacial free energy
ρ_H : density of methane hydrates
L_H : latent heat of the dissociation of pore hydrates
d : pore diameter
T_d : dissociation temperatures of gas hydrates in the bulk phase
T_e : dissociation temperatures of gas hydrates and in confined small pores
MOF : metal organic framework
SG : silica gel
PG : porous glass

REFERENCES

1. H. Davy, *Phil. Trans. Roy. Soc.*, **101**, 155 (1811).
2. T. A. Strobel, C. A. Koh and E. D. Sloan, *Fluid Phase Equilib.*, **261**(1-2), 382 (2007).
3. S. H. Yeon, J. Seol, Y. Park, D. Y. Koh, Y. S. Kang and H. Lee, *J. Am. Chem. Soc.*, **130**(29), 9208 (2008).
4. J. H. Cha, W. Lee and H. Lee, *J. Mater. Chem.*, **19**(36), 6542 (2009).
5. M. D. Max, V. T. John and R. E. Pellenbarg, *Ann. N. Y. Acad. Sci.*, **912**, 460 (2000).
6. H. Lee, J. W. Lee, D. Y. Kim, J. Park, Y. T. Seo, H. Zeng, I. L. Moudrakovski, C. I. Ratcliffe and J. A. Ripmeester, *Nature*, **434**(7034), 743 (2005).
7. D. Y. Kim, Y. Park and H. Lee, *Catal. Today*, **120**(3-4), 257 (2007).
8. J. Y. Lee, B. J. Ryu, T. S. Yun, J. Lee and G. C. Cho, *Ksce J. Civ. Eng.*, **15**(4), 689 (2011).
9. O. Urdahl, A. Lund, P. Mork and T. N. Nilsen, *Chem. Eng. Sci.*, **50**(5), 863 (1995).
10. J. D. Lee and P. Englezos, *Chem. Eng. Sci.*, **61**(5), 1368 (2006).
11. S. H. Yeon, J. Seol, D. Y. Koh, Y. J. Seo, K. P. Park, D. G. Huh, J. Lee

and H. Lee, *Energy Environ. Sci.*, **4**(2), 421 (2011).
12. Y. T. Seo, I. L. Moudrakovski, J. A. Ripmeester, J. W. Lee and H. Lee, *Environ. Sci. Technol.*, **39**(7), 2315 (2005).
13. T. Uchida, S. Takeya, E. M. Chuvilin, R. Ohmura, J. Nagao, V. S. Yakushev, V. A. Istomin, H. Minagawa, T. Ebinuma and H. Narita, *J. Geophys. Res.: Solid Earth*, **109**, B05206 (2004).
14. B. Tohidi, R. W. Burgass, A. Danesh, K. K. Ostergaard and A. C. Todd, *Ann. N. Y. Acad. Sci.*, **912**, 924 (2000).
15. Y. Seo and H. Lee, *J. Phys. Chem. B*, **107**(3), 889 (2003).
16. Y. P. Handa and D. Stupin, *J. Phys. Chem.*, **96**(21), 8599 (1992).
17. T. Uchida, T. Ebinuma and T. Ishizaki, *J. Phys. Chem. B*, **103**(18), 3659 (1999).
18. K. Seshadri, J. W. Wilder and D. H. Smith, *J. Phys. Chem. B*, **105**(13), 2627 (2001).
19. J. W. Wilder and D. H. Smith, *Ind. Eng. Chem. Res.*, **41**(11), 2819 (2002).
20. W. Zhang, J. W. Wilder and D. H. Smith, *AIChE J.*, **48**(10), 2324 (2002).
21. J. W. Wilder and D. H. Smith, *Chem. Eng. Sci.*, **59**(18), 3945 (2004).
22. J. B. Klauda and S. I. Sandler, *Ind. Eng. Chem. Res.*, **40**(20), 4197 (2001).
23. Y. Seo, H. Lee and T. Uchida, *Langmuir*, **18**(24), 9164 (2002).
24. R. Anderson, M. Llamedo, B. Tohidi and R. W. Burgass, *J. Phys. Chem. B*, **107**(15), 3500 (2003).
25. R. Anderson, M. Llamedo, B. Tohidi and R. W. Burgass, *J. Phys. Chem. B*, **107**(15), 3507 (2003).
26. S. P. Kang, J. W. Lee and H. J. Ryu, *Fluid Phase Equilib.*, **274**(1-2), 68 (2008).
27. Y. Seo, S. Lee, I. Cha, J. D. Lee and H. Lee, *J. Phys. Chem. B.*, **113**(16), 5487 (2009).
28. S. Lee and Y. Seo, *Energy Fuels*, **24**, 6074 (2010).
29. S. Lee and Y. Seo, *Langmuir*, **26**(12), 9742 (2010).
30. S. Lee, I. Cha and Y. Seo, *J. Phys. Chem. B*, **114**(46), 15079 (2010).
31. Y. T. Seo, I. L. Moudrakovski, J. A. Ripmeester, J. W. Lee and H. Lee, *Environ. Sci. Technol.*, **39**(7), 2315 (2005).
32. S. Park, S. Lee, Y. Lee, Y. Lee and Y. Seo, *Int. J. Greenhouse. Gas Control*, **14**, 193 (2013).
33. S. P. Kang, W. Jang and Y. Seo, *Abstracts of Papers of the American Chemical Society*, **239**, 101-IEC (2010).
34. A. Eslamimanesh, A. H. Mohammadi, D. Richon, P. Naidoo and D. Ramjugernath, *J. Chem. Thermodyn.*, **46**, 62 (2012).
35. Y. Song, X. Wan, M. Yang, L. Jiang, Y. Liu, B. Dou, J. Zhao and S. Wang, *Energy Fuels*, **27**(6), 3341 (2013).
36. P. Babu, P. Linga, R. Kumar and P. Englezos, *Energy*, **85**, 261 (2015).
37. Y. R. Lee, J. Kim and W. S. Ahn, *Korean J. Chem. Eng.*, **30**(9), 1667 (2013).
38. D. Kim, H.-K. Lim, H. Ro, H. Kim and H. Lee, *Chem. - Eur. J.*, **21**(3), 1125 (2015).
39. S. S. Y. Chui, S. M. F. Lo, J. P. H. Charmant, A. G. Orpen and I. D. Williams, *Science*, **283**(5405), 1148 (1999).
40. A. Buchsteiner, A. Lerf and J. Pieper, *J. Phys. Chem. B.*, **110**(45), 22328 (2006).
41. D. Kim, D. W. Kim, H. K. Lim, J. Jeon, H. Kim, H. T. Jung and H. Lee, *J. Phys. Chem. C*, **118**(20), 11142 (2014).
42. D. Kim, D. W. Kim, H. K. Lim, J. Jeon, H. Kim, H. T. Jung and H. Lee, *Phys. Chem. Chem. Phys.*, **16**(41), 22717 (2014).
43. D. Kim, Y.-H. Ahn and H. Lee, *J. Chem. Eng. Data*, **60**, 2178, (2015).
44. K. Norrish, *Discuss. Faraday Soc.*, **18**, 120 (1954).
45. S. Guggenheim and A. F. K. van Groos, *Geology*, **31**(7), 653 (2003).
46. D. Kim, Y. H. Ahn, S. J. Kim, J. Y. Lee, J. Lee, Y. J. Seo and H. Lee, *J. Phys. Chem. C*, **119**(38), 22148 (2015).
47. T. Uchida, T. Ebinuma, S. Takeya, J. Nagao and H. Narita, *J. Phys. Chem. B*, **106**(4), 820 (2002).

Huen Lee is a Professor in the Department of Chemical and Biomolecular Engineering at the Korea Advanced Institute of Science and Technology in Korea. He received his Ph.D. degree in Chemical Engineering from Northwestern University in 1983. He has endeavored to investigate the scientific perspectives of gas hydrates such as hydrate-based gas capture and separation, hydrogen storage, electrochemical sensors, tuning phenomenon, and some key issues on inclusion chemistry.